Journal of Biomolecular NMR, 4 (1994) 325–333
ESCOM

J-Bio NMR 177

Assignment of NMR spectra of proteins using triple-resonance two-dimensional experiments

Jean-Pierre Simorre, Bernhard Brutscher, Michael S. Caffrey and Dominique Marion*

Institut de Biologie Structurale, CNRS-CEA, 41 Avenue des Martyrs, F-38027 Grenoble Cedex 1, France

Received 23 August 1993
Accepted 25 October 1993

Keywords: Resonance assignments; Multiple-quantum coherence; Proteins; Cytochromes; HNCA; HNCO

SUMMARY

Two-dimensional versions of HNCA and HNCO experiments are described, which provide essentially the same information as the 3D sequence. A multiple-quantum coherence involving either ^{15}N and $^{13}C^{\alpha}$ or ^{15}N and ^{13}CO is created. One of the two frequencies is given by the middle point between the two cross peaks (zero- and double-quantum) and the other by their separation. Quadrature detection can be performed on either nucleus, modifying only the appearence of the 2D spectrum, but not the information content. These experiments, named MQ-HNCA and MQ-HNCO, are illustrated on a (^{15}N,^{13}C) doubly labelled cytochrome c_2 from *Rhodobacter capsulatus* (116 amino acids).

INTRODUCTION

The last few years have seen tremendous advances in the NMR methods for investigating protein structure in solution. The assignment strategy based only on homonuclear 2D NMR (Wüthrich, 1986), which is successfully applied in the case of small proteins (< 100 residues), often fails in the case of larger proteins (100–150 residues), due to extensive chemical shift overlaps and the larger linewidth associated with slow molecular tumbling. Three-dimensional homonuclear (Oschkinat et al., 1988, 1990) and heteronuclear (Fesik and Zuiderweg, 1988; Marion et al., 1989a) NMR seeks to improve the resolution of the spectrum (and thus lessen the first limitation) by increasing the dimensionality of the spectrum. Heteronuclear 3D NMR employs large heteronuclear one-bond couplings for most magnetization transfer steps and is thus less sensitive to large linewidth.

*To whom correspondence should be addressed.

Abbreviations: HMQC, heteronuclear multiple-quantum coherence spectroscopy; HSQC, heteronuclear single-quantum coherence spectroscopy; ZQ, zero quantum; 2Q, double quantum; MQ, multiple quantum; TPPI, time-proportional phase increment.

0925-2738/$ 10.00 © 1994 ESCOM Science Publishers B.V.

Conventional assignment procedures make use of two types of experiments: HOHAHA (in order to identify direct and relayed through-bond connectivities) and NOESY (to obtain sequential through-space connectivities). Exactly the same philosophy can be employed in ^{15}N- or ^{13}C-resolved 3D NMR using HOHAHA-HMQC and NOESY-HMQC (Fesik and Zuiderweg, 1988; Marion et al., 1989; Ikura et al., 1990), where overlaps are resolved by means of the ^{15}N or ^{13}C chemical shift. In addition to this approach which relies on the NOE, heteronuclear 3D NMR can be employed to sequentially assign the backbone nuclei (^{1}H, $^{13}C^{\alpha}$, ^{13}CO and ^{15}N) by means of heteronuclear one-bond and two-bond couplings (Kay et al., 1990,1991). This approach makes use of several 3D experiments, i.e., HNCA, HNCO, HCACO, H(CA)NH and HCA(CO)N (for a review, see Clore and Gronenborn, 1991). These experiments share the following common features: the three dimensions correspond to the three nuclei that are correlated, magnetization originally residing on the protons is transferred to their directly attached ^{15}N or ^{13}C via a heteronuclear polarization transfer sequence and the proton coherences are usually detected at the very end of the experiment in order to benefit from their larger sensitivity.

It is worth noting that, in this 3D approach, the assignment procedure always aims at associating cross peaks sharing a pair of frequencies in two different data sets: for instance, one correlates a cross peak at the frequencies (C^{α}(i),N(i),HN(i)) in the HNCA experiment with one at (CO(i−1), N(i),HN(i)) in the HNCO experiment. One should thus keep in mind that the efficiency of this method (as compared to homonuclear 2D NMR) in fact relies not on the dimensionality of the experiments used but on the identification of frequency pairs, which considerably reduces the number of spectral ambiguities and hence misassignments.

In view of the drawbacks of 3D experiments with respect to 2D (lower resolution and high demand for experimental time and disk storage), one may thus wonder whether the same information cannot be gathered from 2D data sets. Let us summarize the experimental requirements. Final detection of protons is mandatory, in order to capitalize on their higher receptivity. However, to sample two additional frequencies, such as ^{15}N and ^{13}C, a 3D experiment is not necessary. Let us assume that one would want evidence that two spins A and B are J-coupled and identify their chemical shifts ω_A and ω_B. This can be achieved in two different manners:

(1) The frequency ω_A is first labelled, then a coherence is transferred from A to B and finally the frequency ω_B is sampled.

(2) A multiple-quantum AB coherence (actually a combination of ZQ and 2Q coherence) is created first and the two frequencies are measured simultaneously: $\omega_A + \omega_B$ corresponds to a 2Q coherence and $\omega_A - \omega_B$ to a ZQ coherence.

Heteronuclear 3D pulse schemes can in fact be built from two different blocks: HSQC (Bodenhausen and Ruben, 1980) and HMQC (Bax et al., 1983; Bendall et al., 1983). The obtained spectra look quite similar, despite the large differences in pulse sequence design and in relaxation (for example, the HMQC experiment possesses fewer pulses but broader linewidth than the HSQC experiment) (Bax et al., 1990). Inspection of the originally proposed 3D sequences (Kay et al., 1990) shows that the C^{α} frequency in the HNCA sequence and the CO frequency in the HNCO sequence are labelled as zero- and double-quantum coherences, respectively. In both cases, a 180° pulse is applied on the ^{15}N channel, in order to suppress the nitrogen frequency by interchanging the ZQ and 2Q coherences. If this pulse is removed from the ^{13}C evolution period, these two coherences are not mixed and one can thus measure the ^{15}N frequency in addition to the C^{α} or the CO frequency, respectively.

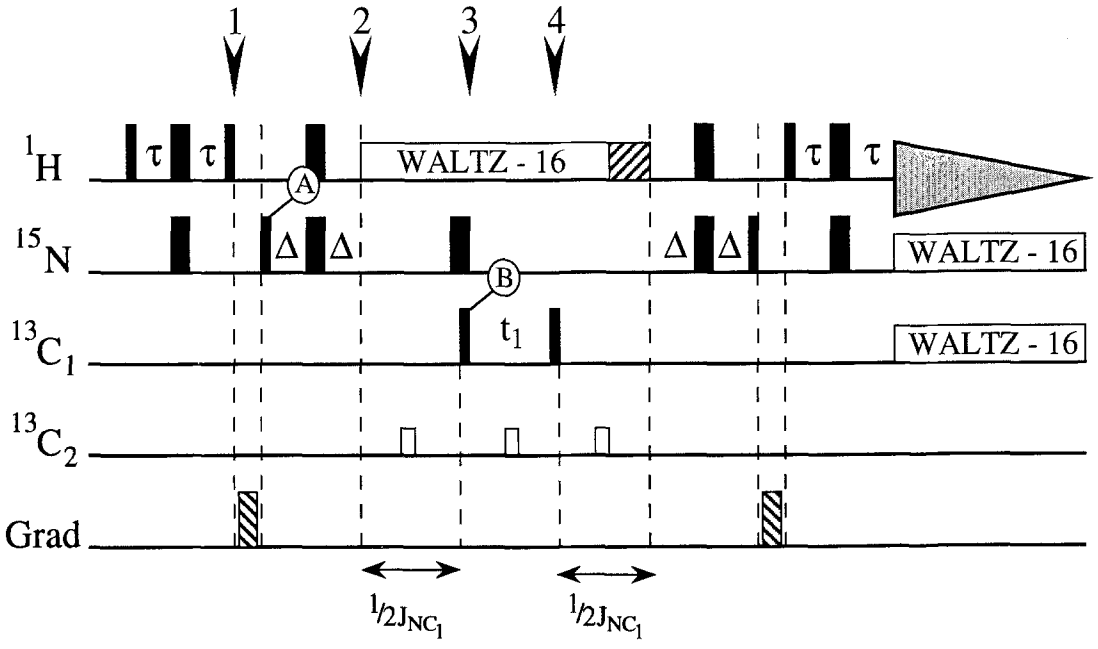

Fig. 1. Pulse sequence used for MQ-HNCO and MQ-HNCA. Experiments were carried out on a Bruker AMX 600 spectrometer with three independent rf channels (^{1}H, ^{13}C and ^{15}N) and a gradient probe. Hard pulses are indicated as filled rectangles (narrow for 90° pulses, wide for 180°) and soft square pulses as open rectangles (only on channel C_2, rf strength $\gamma \times BC_2 = 4.5$ kHz). As discussed in the text, all pulses on channel C_1 (CO in MQ-HNCO and C^α in MQ-HNCA) are hard pulses, and thus excite the other carbon spins (C^α in MQ-HNCO and CO in MQ-HNCA). A linear amplifier (B-LTX-300) is used on the ^{15}N channel and a standard Bruker amplifier on ^{1}H and ^{13}C. The ^{1}H carrier frequency is placed on the water resonance (during the 1.2 s presaturation pulse, not indicated) and then shifted to the middle of the NH resonance. In order to minimize the linear phase gradient, the selective 180° decoupling pulse on C_2 in the middle of t_1 is omitted for the first increment value. As the transverse ^{1}H relaxation is faster than the ^{15}N one, τ is set to 2.25 ms and Δ to 2.7 ms. The ^{1}H spectral width is 3623 Hz for both experiments, whereas the heteronuclear spectral widths are 6036 Hz (for HNCO) and 6579 Hz (for HNCA). The following carrier frequencies are used: HNCO, ^{15}N = 121.8 ppm, $^{13}C^\alpha$ = 60.2 ppm, ^{13}CO = 164.3 ppm; HNCA, ^{15}N = 121.8 ppm, ^{13}CO = 174.8 ppm and $^{13}C^\alpha$ = 48.3 ppm. The duration of the gradient pulse is 200 μs, followed by a recovery time of 400 μs (gradient strength 15–20 G/cm). The proton decoupling (rf strength $\gamma \times B_H = 2.8$ kHz) in the central part of the sequence is followed by a 2-ms trim pulse (hatched rectangle) for residual water suppression. WALTZ decoupling on ^{15}N (for removing the large $^1J_{NH}$) and on ^{13}C (for the long-range J_{CN} was performed during the acquisition (note that the latter may be omitted). Because of the short duration of the selective pulses on C_2 and the large frequency difference between CO and C^α, the frequency change from C_1 to C_2 is done explicitly rather than by introducing a linear phase gradient in a pulse shape. The experimental time for each experiment is approximately 9 h (digital resolution in ω_1 2 × 256 (MQ-HNCO) and 2 × 128 (MQ-HNCA)). Quadrature detection was achieved using the TPPI-States method (Marion et al., 1989b). A half EXORCYCLE (0°, 180°) phase cycling was performed on all 180° pulses and axial peak suppression on the two pulses labelled 'A' and 'B'.

MATERIALS AND METHODS

The above discussion provides the basis for converting the HNCA and HNCO experiments, originally designed as 3D sequences (Kay et al., 1990; Grzesiek and Bax, 1992), into 2D versions, as depicted in Fig. 1. As these experiments rely on the sampling of multiple-quantum coherences, we find it suitable to name them MQ-HNCA and MQ-HNCO. As a result of the large chemical

shift difference between the α-carbons and the carbonyls (>100 ppm), they can be treated as two different nuclei, even if a single rf channel is used on the spectrometer. A single scheme can be employed for the description of these two experiments: Fig. 1 describes the HNCO experiment, in which C_1 = CO and $C_2 = C^{\alpha}$, and the HNCA experiment in the reverse case. We will describe these experiments using the product operator formalism (Sørensen et al., 1983; Van de Ven and Hilbers, 1983) and the following notation: the H_i, N_i, C_{1i} and C_{2i} operators (with i = x,y,z) will refer to ^1H, ^{15}N, $^{13}C_1$ and $^{13}C_2$, respectively.

The experiments start and end with a refocused INEPT transfer (from ^1H to ^{15}N at the beginning and from ^{15}N to ^1H at the end). The transfer delays τ and Δ were optimized from the theoretical value $1/4 \times {}^1J_{NH}$, in order to account for transverse relaxation (see Fig. 1 for details). Filtering of unwanted signals and selection of the longitudinal zz-order (H_zN_z) is done at time 1 by a pulsed field gradient (Bax and Pochapsky, 1992). Between times 2 and 3, dephasing with respect to the C_1 carbon coupling occurs and a ^{15}N-$^{13}C_1$ multiple-quantum (ZQ and 2Q) coherence is thus created by the 90° pulse on C_1. Note that the J_{NC_2} coupling is eliminated between times 2 and 3 by the selective 180° pulse on C_2 and the selectivity of the 90° pulse (at time 3) is thus irrelevant: a hard pulse is thus more convenient as it minimizes the linear phase gradient and does not alter the sensitivity. The end of the sequence is symmetrical to the beginning. The 90° pulse on C_1 (at time 4) converts the multiple-quantum coherence into single-quantum coherence; as discussed below, the phase difference between the two 90° pulses has to be either 0° or 180° in order to yield purely absorptive spectra (peaks with the same phase). Quadrature detection can be done either on ^{15}N or ^{13}C, using standard methods (TPPI, hypercomplex, etc.) on pulses labelled 'A' or 'B'. Further details of the MQ experiment are given in Fig. 1 and the physics of the pulse sequence is discussed in the next section.

RESULTS AND DISCUSSION

Assuming that the 90° pulse on C_1 (at time 3) is aligned along the y-axis, the spin state at the beginning of t_1 can be described as N_xC_{1x}. At the end of the evolution period, it becomes:

$$\begin{aligned} &N_xC_{1x} \cos(\omega N\, t_1) \cos(\omega C_1\, t_1) + N_xC_{1y} \cos(\omega N\, t_1) \sin(\omega C_1\, t_1) + \\ &N_yC_{1x} \sin(\omega N\, t_1) \cos(\omega C_1\, t_1) + N_yC_{1y} \sin(\omega N\, t_1) \sin(\omega C_1\, t_1) \end{aligned} \quad (1)$$

The coherences are precessing only under the influence of the chemical shifts, as the J-coupling between two spins is inactive on the corresponding ZQ and 2Q coherences. The absorptive component of the (±2) Q coherences is described by the operators $N_xC_{1x} + N_yC_{1y}$ and that of the ZQ coherences by $N_xC_{1x} - N_yC_{1y}$. Combinations of the other terms (N_xC_{1y}, N_yC_{1x}) correspond to dispersive components and should thus be cancelled. Thus, if one wants to obtain cross peaks from the ZQ and 2Q coherences, which display the same phase *and* the same intensity, all terms in Eq. 1 except N_xC_{1x} should be eliminated. This goal is actually reached in two independent filtering steps: (a) the final refocused INEPT and (b) the 90° pulse on C_1 at time 4:

(a) One should remember that the refocused INEPT performs a transfer from one spin to another, while selecting only one component of the preexisting transverse magnetization. Thus, depending on the pulse phases, either N_x or N_y (but not both) will be ultimately converted into detectable ^1H magnetization. This filtering on ^{15}N discards either of the two lines of Eq. 1.

(b) The 90° hard pulse at time 3 has created the N_xC_{1x} component. As we want to convert the same component into single-quantum coherence (amplitude modulation), the phase of the 90° pulse at time 4 should be either parallel of antiparallel relative to the previous one. Special attention should be paid to this matter, especially if the decoupling pulse on C_2 (in the middle of the t_1 evolution period) is generated by the same frequency synthesizer as the two hard pulses on C_1 (at times 3 and 4). In fact, a frequency offset for a certain amount of time (T_0) always induces a phase shift (see for instance Guittet et al., 1985) given by:

$$\phi = 2\,\pi\,(\Omega_{C_1} - \Omega_{C_2})\,T_0 \qquad (2)$$

With suitable phase tuning (i.e., optimisation of the time T_0), one can align the two 90° pulses and thus only one first term remains in the two parts of Eq. 1. If the phase difference between the two 90° pulses is ± 90° (rather than 0° or 180°), the ZQ and 2Q peaks will exhibit opposite signs.

In conclusion, a double filtering is done by the refocused INEPT and the 90° pulse on C_1. Thus, a single term of Eq. 1 survives and the ZQ and 2Q cross peaks will show identical amplitude *and* phase. Unfortunately, it is not possible to recover the sensitivity drop resulting from these filterings using the sequences proposed by Palmer et al. (1991), because the two filterings are performed sequentially. Note that, in most of the 2D experiments where a *single* order of coherence is selected, the dephasing between the pulses flanking the evolution period can be compensated by phase correction. This is not feasible in our case.

Let us now discuss in detail the choice of quadrature detection. One should consider both nuclei as independent, as the pulse phases on ^{15}N and $^{13}C_1$ can be changed separately. Quadrature detection (i.e., the sign selection for one nucleus) selects only two out of the four frequencies $\pm\,\omega_{C_1} \pm \omega_N$ present during the evolution period. As the information obtained is unchanged despite a different appearance, performing quadrature detection on either nucleus (^{15}N or $^{13}C_1$) is essentially a matter of convenience. If a quadrature technique (TPPI, hypercomplex, etc.) is applied to the ^{15}N pulse labelled 'A', only one sign will be retained for the ^{15}N frequency (for instance, $\pm\,\omega_{C_1} + \omega_N$). Similarly, quadrature detection on pulse 'B' retains ($+\,\omega_{C_1} \pm \omega_N$). For an easier comparison of HNCA with HNCO, which are sharing a ^{15}N frequency, we find it convenient to select the quadrature detection on ^{15}N. The frequency difference between the ZQ and 2Q peaks will thus be $2 \times (\omega_{CO} - \Omega_N)$ in the MQ-HNCO spectrum and $2 \times (\omega_{C\alpha} - \Omega_{C_1})$ in MQ-HNCA, where Ω_{C_1} is the carrier frequency.

The MQ-HNCO and MQ-HNCA experiments were tested on a (^{15}N,^{13}C) doubly labelled (> 95%) ferrocytochrome c_2 from the photoheterotrophic bacterium *Rhodobacter capsulatus* (concentration ≈ 1 mM). This protein contains 116 amino acids and it functions as a soluble electron carrier between membrane-bound redox centres. The ^1H and ^{15}N resonances have been assigned for the reduced state by 2D ^1H-^1H and ^1H-^{15}N NMR (Gooley et al., 1990). Figure 2 shows the MQ-HNCO and MQ-HNCA spectra of ferrocytochrome c_2, recorded with pulse sequences and parameters given in Fig. 1. Only two residues resonate outside of the spectral regions shown in Fig. 2. Out of 111 theoretically detectable residues (accounting for the N-terminal and the four proline residues), 109 are present in the MQ-HNCO spectrum and 100 in the MQ-HNCA. Comparison of the two spectra clearly shows a narrower ω_1 linewidth for the MQ-HNCO experiment, as the $^1J_{C^\alpha C^\beta}$ coupling (≈ 30 Hz) has not been eliminated in the MQ-HNCA experiment. An expansion of these two spectra is shown in Fig. 3, where all signals

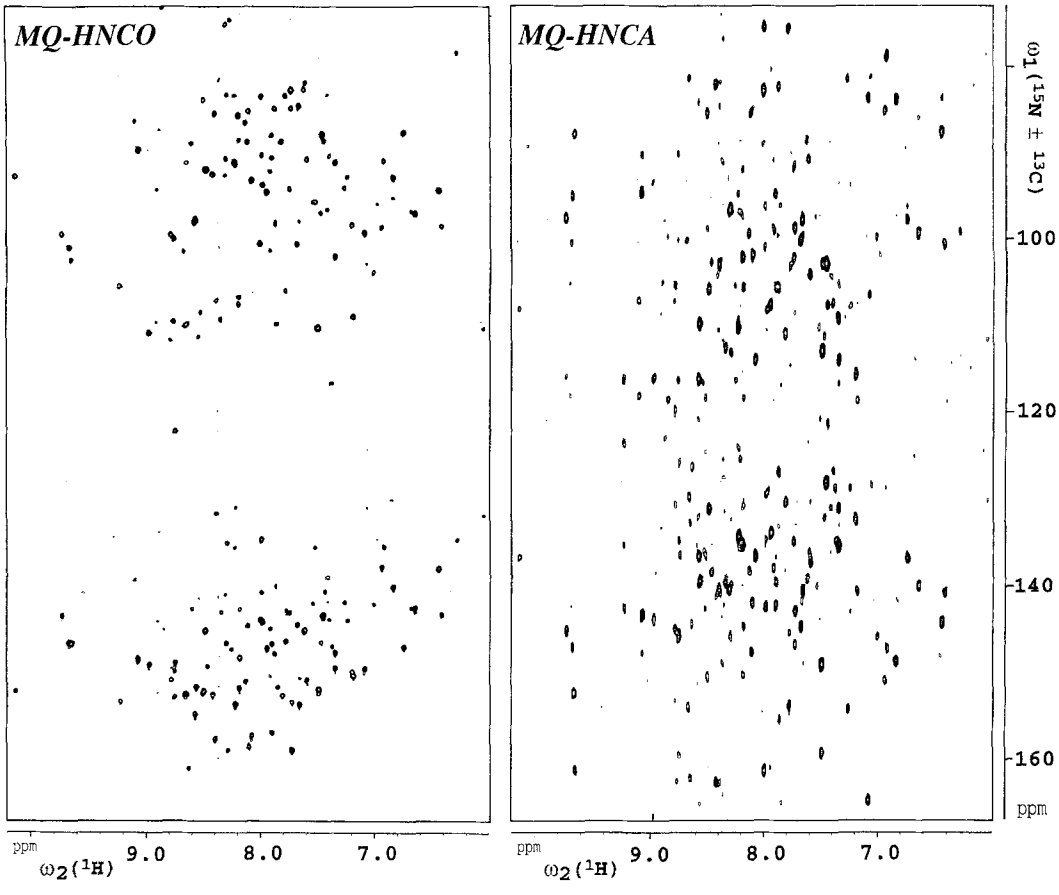

Fig. 2. MQ-HNCO and MQ-HNCA spectra recorded on ferrocytochrome c_2 from *Rhodobacter capsulatus*. A pair of cross peaks is observed for nearly all residues in the protein (see text). The vertical axis indicates the ^{15}N chemical shift. A conversion is necessary [$\times (\gamma C/\gamma N)$] for obtaining the actual ^{13}C chemical shift from the distance between the ZQ and 2Q peaks (along ω_1). For the MQ-HNCO experiment, the C_1 carrier frequency is set at the upfield edge of the carbonyl chemical shift range (164.3 ppm). For MQ-HNCA, the carrier frequency is set at 48.3 ppm, i.e., between the C^α chemical shift range for the glycine residues (from 38.4 to 45.8 ppm in cytochrome c_2) and that of the other residues. Consequently, the specific assignments of the ZQ and 2Q cross peaks (not used here) are interchanged for glycine (as compared to other amino acids).

observed in the region are identified by residue number.

These spectra can be interpreted as follows. Using a HSQC spectrum, recorded under similar conditions, the location of the ^{15}N-^1H cross peaks is identified (marked by a black square in Fig. 3). For each pair of peaks in either the MQ-HNCO or MQ-HNCA spectrum, one then checks that the cross peak in the ^{15}N-^1H HSQC map occurs at the middle point. Thus, the ^1H chemical shift (along ω_2) and the ^{15}N frequency (along ω_1) are given by the middle point (■). In the MQ-HNCO spectrum, the vertical distance between either cross peaks and the middle point is the chemical shift of the carbonyl with respect to the carrier frequency ($\omega_{CO} - \Omega_{C_1}$). In the MQ-HNCA spectrum, the same distance gives the chemical shift of the α-carbon ($\omega_{C^\alpha} - \Omega_{C_1}$). Consequently, in an MQ-HNCO spectrum, the frequencies of the triplet of nuclei (CO(i−1),N(i),NH(i)) are measured

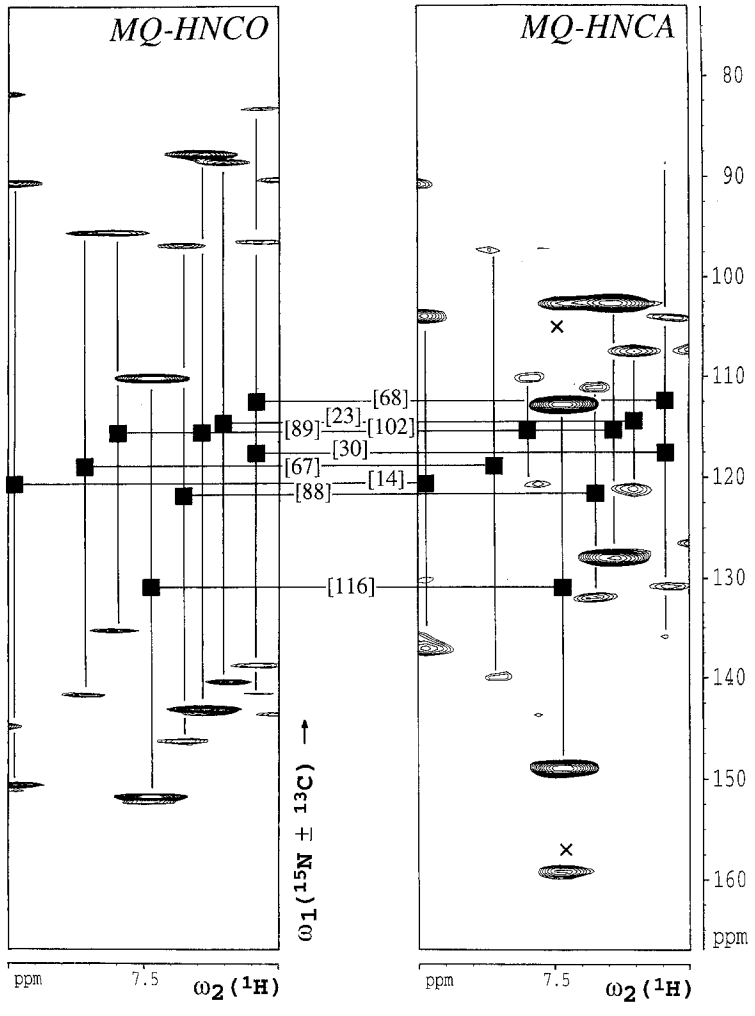

Fig. 3. Expansion of the MQ-HNCA and MQ-HNCO spectra shown in Fig. 2. The peaks are assigned according to residue number and the black squares (■) indicate the location of the cross peaks in the ^{15}N-^{1}H HSQC spectrum (not shown). In the HNCO spectrum the numbers refer to the residues to which the amide ^{15}N and ^{1}H belong (the coupled carbonyl is indeed attached to the preceding residue). The HSQC map is essential for resolving ambiguities due to chemical shift overlaps: without it, the pairing of the ZQ and 2Q peaks would be ambiguous for G30 and T68, owing to the chemical degeneracy of their amide protons. The horizontal lines, which connect the peak pairs between MQ-HNCO and MQ-HNCA, are drawn at the shared ^{15}N chemical shift. In the case of K116, the two crosses in the MQ-HNCA spectrum indicate the weaker cross peaks with the C^{α} of the preceding residue (115), which originate from a transfer via the $^{2}J_{NC}$.

and in the MQ-HNCA spectrum (C^{α}(i),N(i),NH(i)). Figure 3 illustrates how this procedure works: the black square represents the two frequencies which are shared by the two spectra: N(i), NH(i). Note the decisive advantage of performing the quadrature detection on ^{15}N (discussed above), which enables the comparison with the ^{1}H-^{15}N HSQC spectrum.

Let us now compare the 2D MQ experiments with the classical 3D experiments both in terms of sensitivity and resolution. A fair comparison of the sensitivity requires the same overall

experimental time (note that no 3D experiment can be sampled in 9 h with a reasonable resolution). In the 2D MQ spectrum, two peaks are produced and thus a twofold decrease in sensitivity is expected. This drawback is however balanced by moving from three dimensions to two dimensions. For the *same* overall experimental time, the sensitivity of a 2D experiment is always higher than that of the corresponding 3D one: as the number of incremented delays is smaller, the losses due to transverse relaxation are thus minimized. As far as transverse relaxation during the evolution period is concerned, MQ experiments and 3D experiments are quite similar: the relaxation of the MQ coherences is not modified by the presence or absence of a 180° pulse in the middle of the incremented delay.

Assignment of NMR cross peaks implies a reliable discrimination between real signal and noise (or spectral artefacts). Thus, it depends not only on the absolute signal-to-noise (S/N) ratio of the spectrum but also on its a priori known symmetry properties. Consequently, the identification of a pattern of signals can be done at a lower S/N ratio than for an isolated peak. This may distort the sensitivity comparison between 2D MQ experiments and 3D experiments. No symmetry properties can be included in the peak-picking routine for the analysis of 3D HNCA and HNCO spectra. On the other hand, MQ spectra with lower S/N ratio can be used, because of the redundancy of the data: the same distance is to be measured between the ^{1}H-^{15}N HSQC cross peaks and either ZQ or 2Q cross peaks in MQ-HNCA or MQ-HNCO.

As the number of peaks in heteronuclear 3D spectra is very small (one or two peaks per residue), it is common practice to squeeze extensively the spectral width for the indirectly detected nuclei and thus fold resonances. In this respect, MQ experiments are better compromises, although they clearly display lower resolution of cross peaks than the corresponding 3D experiments (2D experiments with two times the number of peaks). However, this apparent limitation can be overcome in two ways: first, peak-picking routines taking into account the symmetry properties (together with the HSQC spectrum) can be used and secondly, remaining ambiguities can be further resolved by the recording of two MQ spectra with a different carrier frequency for the third nucleus (labelled as $^{13}C_1$ in Fig. 1). Finally, it should be emphasised that the spectral resolution (rather than the digital resolution) sets the limits of the 2D MQ experiments, in contrast to 3D experiments. (Typical digital resolution in 3D HNCO and HNCA is 75 Hz/point for the indirectly detected dimensions, which is lower than the corresponding linewidth ($\approx$ 10 Hz for ^{15}N and 30 Hz for ^{13}C.)

On the basis of the previously published ^{1}H and ^{15}N assignments, we have been able to assign nearly all backbone ^{13}C resonances of *Rb. capsulatus* cytochrome c_2. These assignments will be published elsewhere, together with the ^{13}C assignment of the side chains.

CONCLUSIONS

In this paper, we have presented 2D versions of the HNCA and HNCO experiments, which provide the same information as the 3D versions. Consequently, a higher digital resolution can be reached and the experimental time can be reduced. For example, a typical 3D HNCA or HNCO experiment may have a resolution of 100 complex points in the ^{13}C dimension and an experimental time of approximatively three days. In contrast, the 2D MQ-HNCO and MQ-HNCA presented herein have resolutions of 2×256 and 2×128 points in the heteronuclear dimension and an experimental time of 9 h.

Recently, Szyperski et al. (1993) have described a 3D ^{13}C-^{15}N experiment, which also makes use of multiple-quantum coherence for labelling two nuclei simultaneously. The goal of the present work, developed before this paper came to our knowledge, is however different: complete assignment of ^{15}N- and ^{13}C-labelled proteins, using only 2D experiments, similar to the MQ-HNCA and MQ-HNCO described here. Although the assignment strategy is not modified (pairs of frequencies are still compared between several spectra), the extensive reduction of the data storage requirement and experimental time should make these types of experiments very attractive in the near future.

The superiority of the heteronuclear assignment method (based on ^{15}N and ^{13}C) (Kay et al., 1990) over the classical ^{1}H homonuclear method (Wüthrich, 1986) is not intrinsically linked to 3D NMR. We have shown that multiple-quantum correlation techniques enable the correlation of *three* frequencies using a *two-dimensional* experiment and have demonstrated this approach in the case of MQ-HNCA and MQ-HNCO. Extension of this method to other published 3D experiments is currently under investigation in our laboratory.

ACKNOWLEDGEMENTS

M.S.C. is supported by a grant from the Human Frontiers of Science Program. B.B. is the recipient of a Bruker-CEA (France) Ph.D. fellowship. This work was supported by the Centre National de la Recherche Scientifique, the Commissariat à l'Énergie Atomique, the Bruker Company and a US-PHS grant (GM21277) to Prof. Michael Cusanovich (University of Arizona), whose contribution in the preparation of the labelled cytochrome is acknowledged.

REFERENCES

Bax, A., Griffey, R.H. and Hawkins, B.L. (1983) *J. Magn. Reson.*, **55**, 301–315.
Bax, A., Ikura, M., Kay, L.E., Torchia, D.A. and Tschudin, R. (1990) *J. Magn. Reson.*, **86**, 304–318.
Bax, A. and Pochapsky, S.S. (1992) *J. Magn. Reson.*, **99**, 638–643.
Bendall, M.R., Pegg, D.T. and Doddrell, D.M. (1983) *J. Magn. Reson.*, **52**, 81–117.
Bodenhausen, G. and Ruben, D.J. (1980) *Chem. Phys. Lett.*, **69**, 185–192.
Clore, G.M. and Gronenborn, A.M. (1991) *Prog. NMR Spectrosc.*, **23**, 43–92.
Fesik, S.W. and Zuiderweg, E.R.P. (1988) *J. Magn. Reson.*, **78**, 588–593.
Gooley, P.R., Caffrey, M.S., Cusanovich, M.A. and MacKenzie, N.E. (1990) *Biochemistry*, **29**, 2278–2290.
Grzesiek, S. and Bax, A. (1992) *J. Magn. Reson.*, **96**, 432–440.
Guittet, E., Piveteau, D., Delsuc, M.-A. and Lallemand, J.-Y. (1985) *J. Magn. Reson.*, **62**, 336–339.
Ikura, M., Kay, L.E., Tschudin, R. and Bax, A. (1990) *J. Magn. Reson.*, **86**, 204–209.
Kay, L.E., Ikura, M., Tschudin, R. and Bax, A. (1990) *J. Magn. Reson.*, **89**, 496–514.
Kay, L.E., Ikura, M. and Bax, A. (1991) *J. Magn. Reson.*, **91**, 84–92.
Marion, D., Kay, L.E., Sparks, S.W., Torchia, D.A. and Bax, A. (1989a) *J. Am. Chem. Soc.*, **111**, 1515–1517.
Marion, D., Ikura, M., Tschudin, T. and Bax, A. (1989b) *J. Magn. Reson.*, **85**, 393–399.
Oschkinat, H., Griesinger, C., Kraulis, P.J., Sørensen, O.W., Ernst, R.R., Gronenborn, A.M. and Clore, G.M. (1988) *Nature*, **332**, 374–376.
Oschkinat, H., Cieslar, C. and Griesinger, C. (1990) *J. Magn. Reson.*, **86**, 453–469.
Palmer III, A.G., Cavanagh, J., Wright, P.E. and Rance, M. (1991) *J. Magn. Reson.*, **93**, 151–170.
Sørensen, O.W., Eich, G.W., Levitt, M.H., Bodenhausen, G. and Ernst, R.R. (1983) *Prog. NMR Spectrosc.*, **16**, 163–192.
Szyperski, T., Wider, G., Bushweller, J.H. and Wüthrich, K. (1993) *J. Biomol. NMR*, **3**, 127–132.
Van de Ven, F.J.M. and Hilbers, C.W. (1983) *J. Magn. Reson.*, **54**, 512–520.
Wüthrich, K. (1986) *NMR of Proteins and Nucleic Acids*, Wiley, New York, NY.